PASJ: Publ. Astron. Soc. Japan **51**, 603–610 (1999)

FTS Measurements of Submillimeter-Wave Atmospheric Opacity at Pampa la Bola II : Supra-Terahertz Windows and Model Fitting

Satoki MATSUSHITA
Department of Astronomical Science, The Graduate University for Advanced Studies, Nobeyama Radio Observatory, Minamimaki, Minamisaku, Nagano 384-1305*
E-mail (SM): satoki@nro.nao.ac.jp

Hiroshi MATSUO
Nobeyama Radio Observatory, Minamimaki, Minamisaku, Nagano 384-1305*

Juan R. PARDO
George W. Downs Laboratory of Physics, California Institute of Technology, MS 320-47, Pasadena, California 91125, USA
and
Simon J.E. RADFORD
National Radio Astronomy Observatory,† 949 North Cherry Avenue, Tucson, Arizona 85721, USA

(Received 1999 May 10; accepted 1999 July 11)

Abstract

A second observing run aimed to measure the millimeter and submillimeter-wave (150–1500 GHz or 2 mm–200 μm) atmospheric opacity was carried out with a Fourier Transform Spectrometer (FTS) at Pampa la Bola, 4800 m above sea level in northern Chile. We obtained high transmission spectra, showing up to $\sim$ 67% transmission at submillimeter-wave windows. The observed spectra can be well modeled by newly developed radiative-transfer calculations. Correlations between 220 GHz and submillimeter-wave opacities were reanalized, including the new data set. The results show almost identical trends as the ones resulting from the first measurements. We also identified supra-terahertz windows (located around 1035 GHz, 1350 GHz, and 1500 GHz), which could not be seen in our first measurements. Opacity correlations between the 220 GHz and these new windows are derived for the first time. Combined with a statistical study of the 225 GHz opacity data of the Chajnantor site (7 km apart from Pampa la Bola), it is estimated that submillimeter-wave observations can be done with zenith opacity less than 1.0 (at the most transparent frequency in those windows) for about 50% of the winter season.

Key words: Atmospheric effects — Instrumentation: spectrometer — Site testing — Submillimeter

1. Introduction

The submillimeter-wave region of the electromagnetic spectrum is the most suitable for astrophysical research, such as dust emission from young stellar objects and primeval galaxies, and hot molecular gas from active star-forming regions. At the beginning of the 21st century, a large millimeter and submillimeter-wave interferometer with high sensitivity and high angular resolution is planned to be built at a high-altitude site of the Atacama desert, Chile. This array is to be a combined effort of different communities: Japanese LMSA (Large Millimeter and Submillimeter Array; Ishiguro 1998), American MMA (Millimeter Array; Brown 1998), and European LSA (Large Southern Array; Guilloteau 1998) projects. The prospective site for the LMSA project has been Pampa la Bola, at 4800 m above sea level. The one for the MMA and LSA projects has been Chajnantor, at 5000 m of altitude, 7 km apart from Pampa la Bola. Since submillimeter-wave observations suffer from strong and rapidly varying water-vapor absorption, astronomical observatories operating at these wavelengths should be built

* Nobeyama Radio Observatory (NRO) is a branch of the National Astronomical Observatory, an inter-university research institute operated by the Ministry of Education, Science, Sports and Culture.

† National Radio Astronomy Observatory (NRAO) is a facility of the National Science Foundation operated under cooperative agreement by Associated Universities, Inc.

at dry, high-altitude sites. There are some submillimeter-wave observatory sites currently in use or under site testing, such as Mauna Kea, Hawaii (e.g., Masson 1994; Serabyn et al. 1998), the South Pole (e.g., Chamberlin et al. 1997), and the Atacama desert of northern Chile (e.g., Hirota et al. 1998; Matsuo et al. 1998a).

At Pampa la Bola, Fourier Transform Spectrometer (FTS) measurements were performed by Matsuo et al. (1998a; hereafter Paper I) during 1997 September 5 and 12. They revealed opacity correlations between 220 GHz and all the submillimeter-wave windows. Unfortunately, the weather conditions were limited during those measurements. Other measurements (220 GHz and 492 GHz atmospheric opacity measurements done by Kohno et al. 1995 and Hirota et al. 1998, and 11 GHz radio seeing measurements) were also made at Pampa la Bola; these results are briefly summarized in Paper I.

With the purpose of obtaining atmospheric spectra under better weather conditions, we carried out the second observing run at Pampa la Bola using the same technique. This time, the atmospheric conditions were among the best for the site, and we also measured some transmission in several supra-terahertz windows (section 3). We performed a radiative transfer calculation to fit the observed transmission spectrum (section 3). We present opacity correlation diagrams (section 4), and estimate the fraction of time with good submillimeter-wave observing conditions at Pampa la Bola–Chajnantor area (section 5).

2. Measurements

Millimeter and submillimeter-wave atmospheric opacity measurements at Pampa la Bola (northern Chile, the Atacama desert, 4800 m altitude) were carried out using a Martin–Puplett type Fourier transform spectrometer (Martin, Puplett 1970) and an InSb bolometer. The data presented in this paper were recorded continuously from 6 pm, 1998 June 16, and stopped by a problem in a mirror drive circuit at 4 am, June 18, in Chilean local time (UT − 4 hr). The weather conditions were fine with clear skies during most of the observing run, but in the morning of June 18, there were thick clouds in the sky. The beam size was about 10°, and the apodized frequency resolution was 0.3 cm^{-1} (∼ 10 GHz). Atmospheric emission spectra were obtained at different airmasses of 1.0, 1.5, 2.0, 2.5, and 3.0 by rotating a tipping mirror outside of the spectrometer. Two independent opacity measures were obtained; one is given from the temperature spectra at the zenith (temperature measurements); the other is provided by tipping scans (tipping measurements). A tipping measurement with the FTS including temperature calibrations was made every 14 minutes. The absolute-brightness temperature of the atmosphere was calibrated using a blackbody (Eccosorb AN74) at liquid-nitrogen temperature (∼ 73 K at 4800 m altitude) and another one at ambient temperature between every tipping scan. Calibration signals during the whole period were stable within 1%. The ambient temperature was monitored with a weather station. The cold calibrator was covered with a thin black polyethylene film to prevent rapid evaporation of liquid nitrogen and a possible effect of solar radiation. Absorption and reflection loss of the polyethylene was taken into account in further analysis. Further details on the instruments, measurements, and calibrations are described in Paper I.

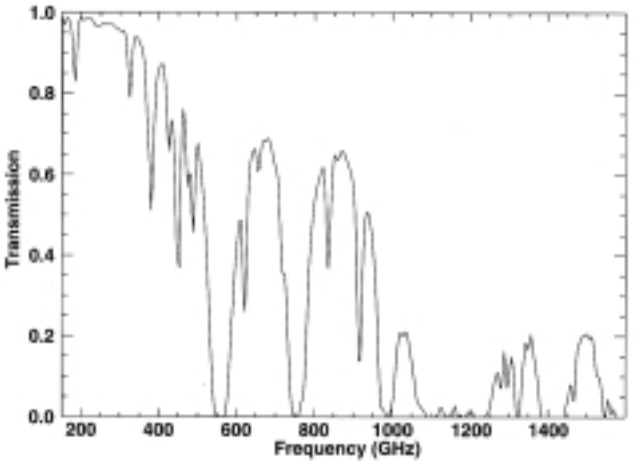

Fig. 1. Atmospheric transmission spectrum obtained from the tipping measurement (< 450 GHz) and the temperature measurement (> 450 GHz). The tipping scan used for this figure was taken between 10:19 and 10:33, 1998 June 17, in Chilean local time (UT − 4 hr).

3. Atmospheric Transmission Spectra

On the morning of 1998 June 17, we recorded the best atmospheric transmission spectra during the observing run (figure 1). In this figure (and also in further analysis), the transmission was obtained from tipping measurements for frequencies of up to 450 GHz, and from temperature measurements above 450 GHz (see Paper I for details). The opacity measured at 220 GHz was ∼ 0.016 (∼ 98% in transmission), and those of the submillimeter-wave windows (650 GHz and 850 GHz windows) were as low as 0.40, corresponding to transmissions of about 67%.

We also identified three main atmospheric windows above 1 THz, which were first measured by Paine and Blundell (1999). The frequency ranges of these windows are ∼ 1000–1100 GHz, 1250–1400 GHz, and 1450–1600 GHz. The opacities at the center of these windows were similar (about 1.6), which is about 20% in

Table 1. Frequencies and its astronomical and/or atmospheric interests.

Frequency	Interests
345 GHz	Center of the window, CO ($3 \rightarrow 2$)
410 GHz	Center of the window
492 GHz	[C I]($^3P_1 \rightarrow ^3P_0$)
675 GHz	Center of the window
691 GHz	CO ($6 \rightarrow 5$)
809 GHz	[C I]($^3P_2 \rightarrow ^3P_1$), CO ($7 \rightarrow 6$) [807 GHz]
875 GHz	Center of the window
922 GHz	CO ($8 \rightarrow 7$)
937 GHz	Center of the window
1035 GHz	Center of the window, CO ($9 \rightarrow 8$) [1037 GHz]
1350 GHz	Center of the window, CO ($12 \rightarrow 11$) [1382 GHz]
1500 GHz	Center of the window, [N II]($^3P_1 \rightarrow ^3P_0$) [1471 GHz], CO ($13 \rightarrow 12$) [1497 GHz]

transmission. However, due to limited sensitivity around 1500 GHz and offset errors in the phase correction of the Fourier-transformed spectra, there are some systematic errors in the transmission spectra in the 1450–1600 GHz window (it could be up to 10% in transmission). The frequency range between the atmospheric windows is still less sensitive because of water vapor absorption inside the spectrometer, itself, where the error could be larger. During the observing run, we also carried out side-by-side measurements with another FTS experiment at Chajnantor by Paine and Blundell (1999), and the measured transmission spectra showed very good correspondence to each other within an accuracy of $\lesssim 1\%$ in the 650 GHz and 850 GHz windows.

Since our atmospheric transmission spectra cover a wide frequency range (150–1500 GHz or 2 mm–200 μm), they can be good samples to compare with radiative-transfer atmospheric models. We performed radiative-transfer calculations using the model ATM (Atmospheric Transmission at Microwaves; Pardo 1996) to fit the spectra. This model was also used to analyze fine calibrated FTS spectra (within 1% in transmission) with 200 MHz frequency resolution from Mauna Kea (Serabyn 1999, private communication). For the calculations, we included the effect of water vapor, oxygen, and other minor gas absorption lines, and water vapor and dry air continuum absorptions. The best fit to the data with these absorption components is shown in figure 2 (Plate 24).

As can be seen in the figure, the model fits very well with the observed spectrum with only three free parameters [the precipitable water vapor column (pwvc) above the site, and the strength and frequency dependence of the water vapor continuum], except for frequencies higher than 1350 GHz, where the measurement suffers from systematic errors. The fit results in a pwvc of 0.252 mm. Smoothing was applied to the model in order to match the actual frequency resolution of the data. Ozone absorption occurs in the stratosphere where the temperature is different from that of the tropospheric water vapor and oxygen that dominate the overall shape of the spectrum. As a result, ozone absorption is underestimated by the calibration procedure that approximates the atmospheric temperature to the ambient (ground level) temperature. A correction factor of 0.7 was applied to the amount of ozone predicted for the site by atmospheric models in order to compensate for this effect in the fitting (Serabyn et al. 1998). We can also see that the fit has large residuals near to the atmospheric O_2 resonances. The larger scale height of the O_2 profile compared to that of H_2O results in an underestimation of the opacity in the vicinity of O_2 lines by the calibration procedure of Paper I. Thus, the multilayer radiative transfer model will always be in disagreement with the measurement. This instrumental effect is described in detail in Serabyn et al. (1998).

4. Opacity Correlations between Millimeter and Submillimeter-Waves

Scatter plots between 220 GHz opacity and 345, 410, 492, 675, 691, 809, 875, 922, 937, 1035, 1350, and 1500 GHz opacities are shown in figures 3a–l. The plots contain both the new data which were obtained under stable weather conditions between 6 pm, 1998 June 16 and 10 pm, June 17 (filled circles) and those from Paper I (open circles). The selected frequencies are either located at the center of atmospheric windows and/or are frequencies of special astronomical interest, which are summarized in table 1. For each diagram, a linear regression, $\tau_f = a\tau_{220} + b$, was performed and plotted. The resulting coefficients are listed in table 2. The new data complete the scatter plots in the region of low opacities, and the

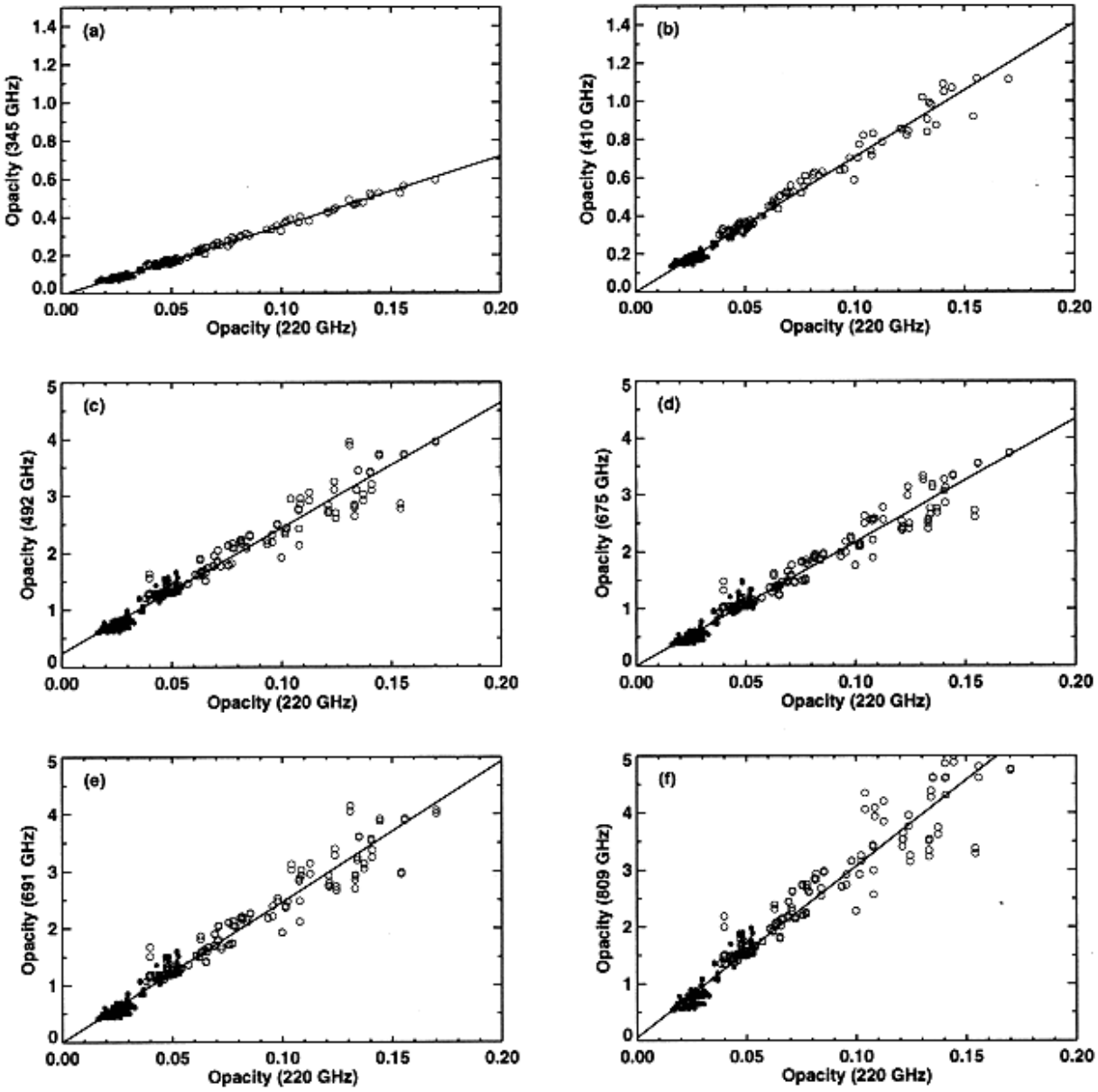

Fig. 3. Correlation diagrams between 220 GHz opacities and submillimeter-wave opacities. The filled circles indicate new data taken between 6 pm, 1998 June 16 and 10 pm, June 17, and open circles indicate data from Paper I which were taken between the 5 and 12 of 1997 September. The solid lines of each figure indicate the calculated linear regressions. The dashed lines in (h)–(j) indicate the same correlation coefficient, but with no zero-point offset. The solid lines in (k)–(l) indicate the calculated linear regressions with no zero-point offset.

results are consistent with those of Paper I. Comparisons between our data and other published measurements are discussed in Paper I.

We also present the results of a regression analysis for frequencies above 900 GHz for the first time. These windows tend to have large proportionality (a) coefficients, meaning that a small change in the weather conditions causes a large variation in the transparency. Since we have fewer data points at 1350 GHz and 1500 GHz and the data ranges are narrow, the linear regressions for these frequencies were performed with no zero-point offset (i.e., $\tau_f = a\tau_{220}$).

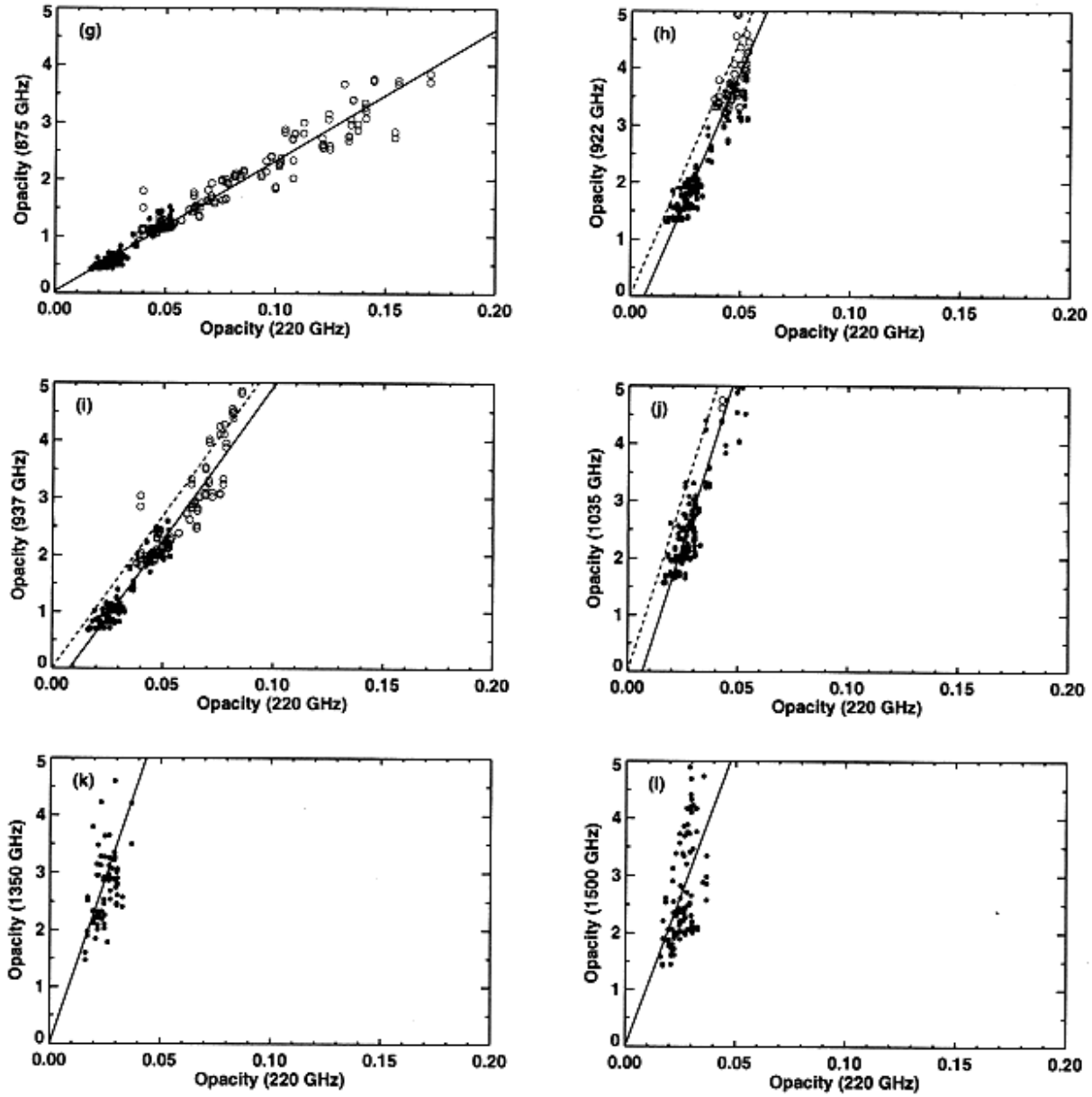

Fig. 3. (Continued)

We also obtained quite different scatter plots (figures 4a–f) between 10 pm, 1998 June 17 and 4 am, June 18. Because of their anomalous behavior, the data are excluded from figure 3, and are plotted separately in figure 4 (dashed lines in figure 4 are the same correlations as in figure 3). These data subsets show lower correlation coefficients and larger zero-point offsets than the 'normal' correlations shown by the dashed lines, which means that although the millimeter opacities change greatly, the submillimeter opacities do not. The empirical water vapor continuum absorbs stronger in the higher frequency region than in the lower frequency region [see figure 2 (Plate 24)]. On the other hand, the liquid-water component (cloud or fog) absorbs more effectively at lower frequencies for a given particle-size distribution (e.g., Liebe et al. 1991; Ray 1972). Therefore, a variation in the quantity of the liquid-water component of the atmosphere mainly causes a change in the lower frequency opacity. Thus, in the opacity correlations with 220 GHz and higher frequencies, the liquid-water com-

Table 2. Proportionality coefficients and offsets in the correlations between 220 GHz and submillimeter-wave opacities.*

Frequency	a	b	σ [%]†
345 GHz	3.62 ± 0.03	−0.009 ± 0.002	9
410 GHz	7.05 ± 0.08	−0.001 ± 0.005	10
492 GHz	22.0 ± 0.3	0.24 ± 0.02	11
675 GHz	21.7 ± 0.2	0.00 ± 0.02	14
691 GHz	24.7 ± 0.3	0.00 ± 0.02	15
809 GHz	30.2 ± 0.4	0.05 ± 0.03	16
875 GHz	23.0 ± 0.3	0.03 ± 0.02	14
922 GHz	90 ± 3	−0.6 ± 0.1	16
937 GHz	53.7 ± 0.9	−0.43 ± 0.04	15
1035 GHz	123 ± 5	−0.8 ± 0.2	18
1350 GHz§	115 ± 29	—	25
1500 GHz§	105 ± 32	—	30

*$\tau_f = a\tau_{220} + b$.
†Standard deviation from a linear correlation normalized by the opacity ($\Delta\tau_f/\tau_f$).
§The linear regressions were calculated with no zero point offset (i.e., $\tau_f = a\tau_{220}$).

ponent makes the slope of the correlations change, their zero points to offset and the standard deviations to be larger. This trend can be seen in figure 4, suggesting that these correlations would show the effect of liquid-water absorption.

The zero-point offsets (b) in the windows above 900 GHz also have large values (figures 3h–j). This behavior can also be the effect of liquid-water absorption. We indicate by the dashed lines in figures 3h–j the original linear regressions, but with no zero-point offsets. Almost all of the plotted points are located in the region of 220 GHz opacities larger than those of these dashed lines (this can also be seen in figure 4). These examples also support the existence of liquid-water absorption, as indicated above. The quantitative analysis of the effect of liquid-water absorption is under way.

Table 3. The fraction of time of the low opacity conditions in submillimeter-wave region.*

Season†	$\tau^{\S}_{\rm SMM} \lesssim 0.6$ $\tau^{\P}_{\rm STHz} \lesssim 3$	$\tau^{\S}_{\rm SMM} \lesssim 1.0$
Summer	7%	24%
Winter	15%	50%
Year	11%	37%

*Results are based on the opacity data with 225 GHz tipping radiometer installed at Chajnantor in 1995 April (Radford, Holdaway 1998).
†Summer is from November to April, and winter is from May to October.
§Opacity of 675 GHz and 875 GHz windows.
¶Opacity of 1035 GHz, 1350 GHz, and 1500 GHz windows.

5. Submillimeter-Wave Observing Conditions at Pampa la Bola–Chajnantor Area

Using the correlations between 220 GHz opacity and submillimeter-wave opacities derived above, and the data continuously recorded by the 220 GHz tipping radiometer (Kohno et al. 1995), we can estimate the fraction of time of good submillimeter-wave observing conditions. A side-by-side experiment involving the 220 GHz tipping radiometer and our FTS indicates that the 220 GHz opacity data on both instruments show good agreement, within 1% in transmission (Matsuo et al. 1998b). Because of a limited amount of data from the radiometer at Pampa la Bola for a statistical study (available since 1997 September), we used data from the 225 GHz tipping radiometer at Chajnantor site (Radford, Holdaway 1998), which has been operated since 1995 April. Side-by-side measurements were also performed involving the Chajnantor site and the Pampa la Bola site radiometers; the resultant opacity data show good agreement to each other (K. Kohno 1997, private communication). In table 3, the submillimeter observing conditions are estimated from the correlations in table 2 and 225 GHz opacity statistics from Radford and Holdaway (1998).

The fraction of time of 225 GHz opacity below 0.03 (corresponding to a maximum transmission at submillimeter-wave windows of $\gtrsim 50\%$) in the Pampa la Bola–Chajnantor area is $\sim 15\%$ in winter and $\sim 7\%$ in summer. Under this condition, the supra-terahertz windows open with minimum opacities of less than 3.0. The fraction of time of 225 GHz opacity below 0.05 (submillimeter-wave opacity of $\lesssim 1.0$) is $\sim 50\%$ and $\sim 24\%$ in the winter and summer, respectively. In Mauna

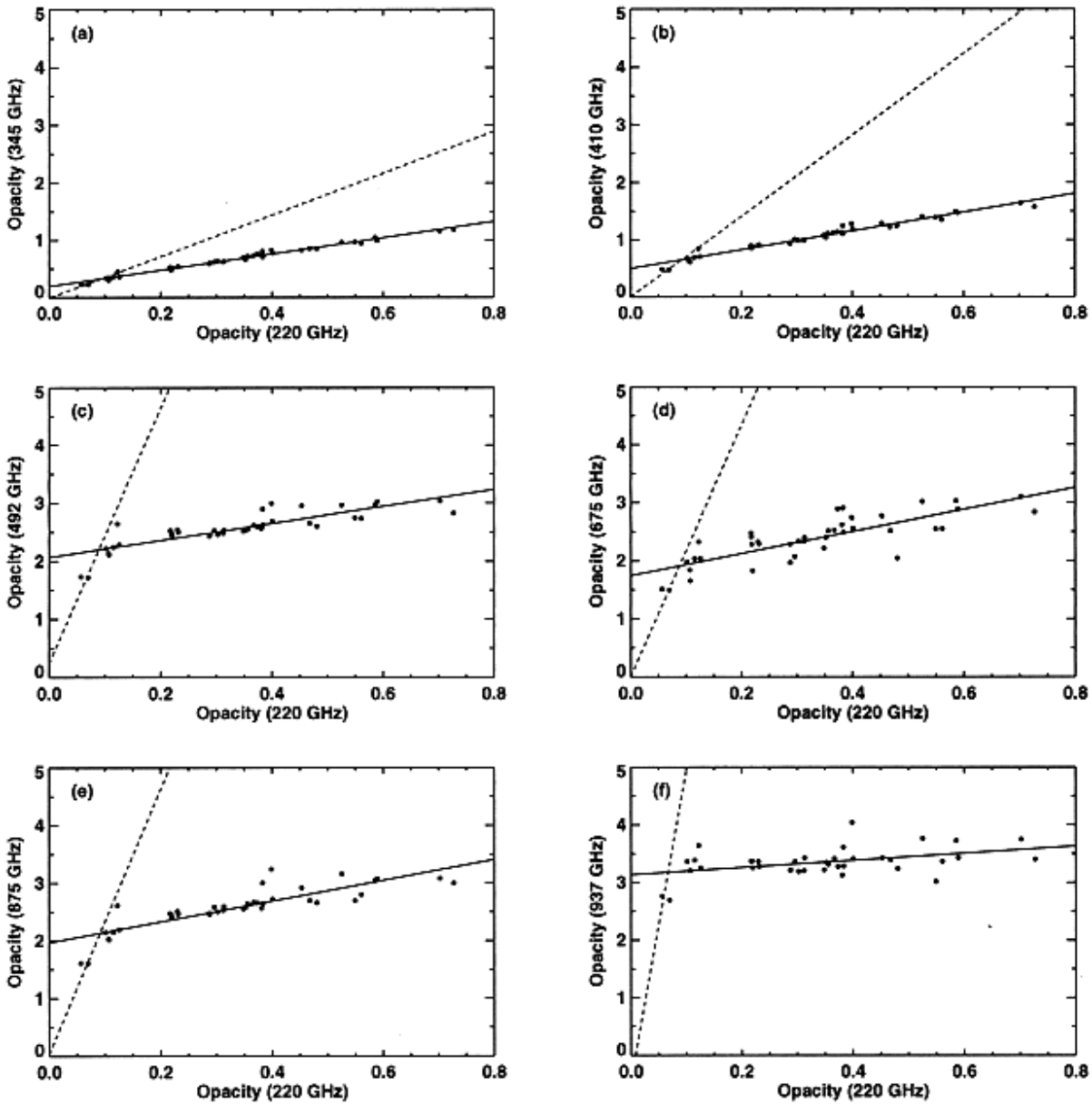

Fig. 4 Correlation diagrams between 220 GHz opacities and submillimeter-wave opacities which may be extremely affected by the liquid water absorption. The data were taken between 10 pm, 1998 June 17 and 4 am, June 18 in Chilean local time (UT − 4 hr). In these figures, submillimeter-wave opacities of 345, 410, 492, 675, 875, and 937 GHz are indicated. The solid lines of each figure indicate the calculated linear regressions. The dashed lines are the 'normal' correlation shown in figures 3.

Kea, 225 GHz opacity below 0.05 occurs $\lesssim 25\%$ in a year (Masson 1994), so that the Pampa la Bola–Chajnantor area is a better site for the submillimeter observations than Mauna Kea in terms of atmospheric opacity conditions.

6. Conclusions

The second FTS observing run at Pampa la Bola has provided high submillimeter-wave atmospheric transmission spectra, including supra-terahertz windows. The observed spectra can be well modeled by newly developed radiative-transfer calculations. Correlations be-

tween 220 GHz opacity and submillimeter-wave opacities are consistent with the results of our previous FTS measurements performed in 1997. Correlations between the opacities at 220 GHz and those of the supra-terahertz windows were obtained for the first time. Using these correlations and 225 GHz long-term opacity measurements, we estimated that about half of a winter-season submillimeter-wave observations can be done under a zenith opacity of less than ~ 1 (at window minima). We also indicated the existence of absorption by the liquid-water components (cloud or fog). To confirm this effect, it would be important to compare the data with a model including the liquid-water component (currently under development). In addition, because this component would also affect the phase fluctuations, a comparison between the opacity and the phase fluctuations would also be important. These will be addressed in forthcoming papers.

The authors are grateful to A. Otarola of European Southern Observatory, and G. Valladares of National Radio Astronomy Observatory for supporting this site test experiment. We thank S. Paine and R. Blundell of Smithsonian Astrophysical Observatory for the support of side by side measurements at Chajnantor. Success of the experiment was due to T. Kamazaki, N. Kuno, and other people from the LMSA group and Nobeyama Radio Observatory. Thanks are also due to K. Shirawachi of JASCO company for quick support from Japan during the FTS operations. We also thank T. Manabe of Communications Research Laboratory and the referee for helpful discussions and comments. SM is financially supported by the Research Fellowships of the Japan Society for the Promotion of Science (JSPS) for Young Scientists. J. R. Pardo is currently supported by U.S. NSF grant # ATM-9616766. He also gratefully acknowledges partial support from NSF grant # AST-9615025, the NASA-Goddard Institute for Space Studies, the Observatoire de Paris-Meudon, French CNES [Décision d'aide à la recherche (795/98/CNES/7492)] and Météo-France for the development of his research. This work was supported by the Inter-Research Centers Cooperative Program of the JSPS.

References

Brown R. 1998, in Advanced Technology MMW, Radio, and Terahertz Telescopes, ed T.G. Phillips, Proc. SPIE 3357, p231

Chamberlin R.A., Lane A.P., Stark A.A. 1997, ApJ 476, 428

Guilloteau S. 1998, in Advanced Technology MMW, Radio, and Terahertz Telescopes, ed T.G. Phillips, Proc. SPIE 3357, p238

Hirota T., Yamamoto S., Sekimoto Y., Kohno K., Nakai N., Kawabe R. 1998, PASJ 50, 155

Ishiguro M. 1998, in Advanced Technology MMW, Radio, and Terahertz Telescopes, ed T.G. Phillips, Proc. SPIE 3357, p244

Kohno K., Kawabe R., Ishiguro M., Kato T., Otarola A., Booth R., Bronfman L. 1995, Nobeyama Radio Observatory Technical Report, No. 42

Liebe H.J., Huttford G.A., Manabe T. 1991, Intern. J. Infrared Millimeter Waves 12, 659

Martin D.H., Puplett E.F. 1970, Infrared Phys. 10, 105

Masson C.R. 1994, in Astronomy with Millimeter and Submillimeter Wave Interferometry, ed M. Ishiguro, W.J. Welch, ASP Conf. Ser. 59, p87

Matsuo H., Sakamoto A., Matsushita S. 1998a, PASJ 50, 359 (Paper I)

Matsuo H., Sakamoto A., Matsushita S. 1998b, in Advanced Technology MMW, Radio, and Terahertz Telescopes, ed T.G. Phillips, Proc. SPIE 3357, p626

Paine S., Blundell R. 1999, in Programs and Abstracts of the USNC/URSI Meeting, p205

Pardo J.R. 1996, Ph.D. Thesis, Université Pierre et Marie Curie-Universidad Complutense de Madrid

Radford S.J.E., Holdaway M.A. 1998, in Advanced Technology MMW, Radio, and Terahertz Telescopes, ed T.G. Phillips, Proc. SPIE 3357, p486

Ray P.S. 1972, Appl. Opt. 11, 1836

Serabyn E., Weisstein E.W., Lis D.C., Pardo J.R. 1998, Appl. Opt. 37, 2185

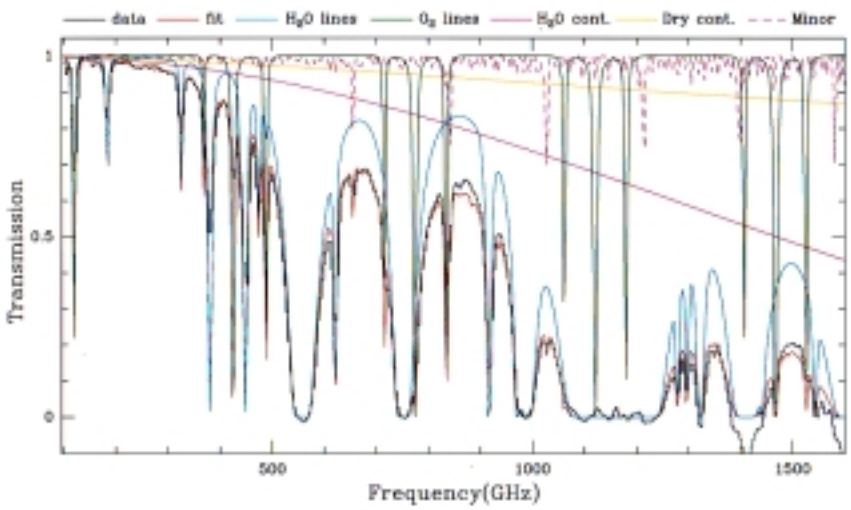

Fig. 2. Theoretical radiative transfer calculation result overplotted on the atmospheric transmission spectrum, as shown in figure 1. Black line: Observed spectrum (same as figure 1). Red line: The best-fitted radiative transfer model of the observed spectrum. Blue line: Water-vapor absorption lines. Green line: O_2 absorption lines. Purple solid line: Water-vapor continuum absorption. Yellow line: Dry air continuum absorption. Purple dashed line: Minor gas absorption lines.